Flow map composition to identify coherent structures

18th International Symposium on Flow Visualization
Zurich, Switzerland, June 26-29, 2018

Flow Map Composition to Identify Coherent Structures

Steven L. Brunton

Abstract

The flow map of a dynamical system plays a major role in the computation of finite-time Lyapunov exponents (FTLE), and the Perron-Frobenius and Koopman operators, each of which are important for visualizing coherent structures and quantifying uncertainty in unsteady fluid dynamics. However, the flow map calculation is expensive, both in terms of computation time and memory requirements. In this work, we continue to develop the theory of flow map composition, whereby long-time flow maps are constructed as the composition of multiple short-time flow maps to eliminate redundant computations. In particular, we provide an error analysis and investigate flow map composition for simple discrete-time maps (e.g., logistic and tent maps) as well as for fluid flow data.

1 Introduction

Integrating initial conditions through a dynamical system provides insight into the geometric organization of trajectories, aiding in the identification of coherent structures and separatrices in the flow. The resulting *flow map* may be approximated numerically on a grid of initial conditions from velocity fields obtained either via simulations or experimentally, making these methods *data-driven*. Flow maps are central to the computation of almost invariant sets (AIS) [1], finite-time Lyapunov exponents (FTLE) and the resulting Lagrangian coherent structures (LCS) [2, 3, 4, 5], and the propagation of a probability density through a dynamical system. There are many compelling examples, including animal predation [6], three-dimensional turbulence [7], geophysical flows [8, 4], and cardiovascular flows [9]. FTLE fields have also been used extensively to study the motion of inertial particles [10, 11], including airborne microbes [12, 13], transport in the ocean [14], plankton fleeing predators [15], urban flows [16, 17], and hurricane dynamics [18].

For time-varying dynamics, it may be necessary to compute a time-series of flow maps to visualize these structures evolving in time (see Fig. 1 for frames in a movie of flow past a pitching plate, simulated using the immersed boundary projection method [19, 20]). This is computationally expensive, and there is significant overlap in the particle integrations from neighboring flow map computations. The *fast* FTLE method [21] speeds up neighboring flow map computations by computing and storing intermediate flow maps, which are used to construct longer-time flow maps by composition; the earlier phase-flow method provides similar speed-ups for autonomous systems [22]. Flow map composition has also been applied to generalized polynomial chaos (gPC) [23, 24, 25, 26], extending it for long-time integrations [27]. In this work, flow map composition is investigated further on a class of discrete dynamical systems, and an in-depth error analysis is provided.

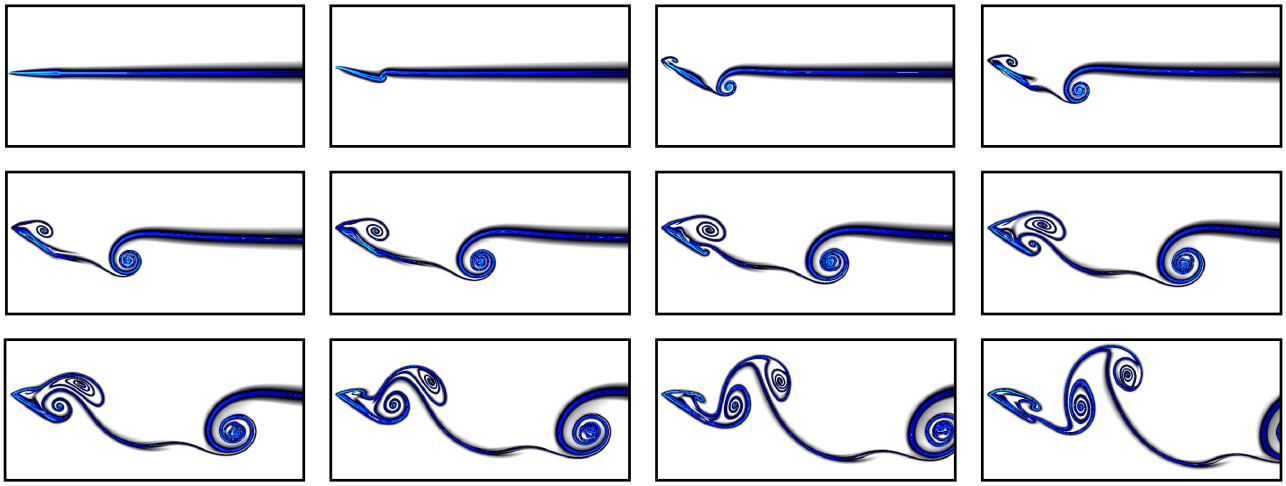

Figure 1: Flow visualization with finite time Lyapunov exponents for flow past an airfoil at Reynolds number 100 after a rapid pitch-up maneuver.

2 Background on flow map composition

Consider a dynamical system on a domain $\mathcal{D} \subseteq \mathbb{R}^n$:

$$\dot{x} = f(x,t) \tag{1}$$

where $x \in \mathcal{D}$ and $f : \mathcal{D} \times \mathbb{R} \to \mathbb{R}^n$ is Lipschitz. For an initial condition, $x(t_0) = x_0$, trajectories are denoted $x(t; t_0, x_0)$.

Definition 2.1. The *flow map* $\phi_{t_0}^{t_f} : \mathcal{D} \to \mathcal{D}$ maps x_0 to $x(t; t_0, x_0)$ and is given by:

$$\phi_{t_0}^{t_f} : x(t_0) \mapsto x(t_0) + \int_{t_0}^{t_f} f(x(\tau), \tau) d\tau. \tag{2}$$

Definition 2.2. The *finite-time Lyapunov exponent* (FTLE) σ is given by:

$$\sigma = \frac{1}{|t_f - t_0|} \log \sqrt{\lambda_{\max}\left(\Delta\right)} \tag{3}$$

where $\Delta = \left(\mathbf{D}\phi\right)^* \left(\mathbf{D}\phi\right)$ is the Cauchy-Green deformation tensor, and $\mathbf{D}\phi = \frac{\partial \phi_i}{\partial x_j}$ is the flow map Jacobian.

Remark 1. The maximum singular value of the flow map Jacobian, $\mathbf{D}\phi_{t_0}^{t_f}$, is given by the following operator norm:

$$\|\mathbf{D}\phi_{t_0}^{t_f}\|_2 := \max_{\epsilon \neq 0} \frac{\|\mathbf{D}\phi_{t_0}^{t_f} \cdot \epsilon\|_2}{\|\epsilon\|_2} = \exp(\sigma |t_f - t_0|). \tag{4}$$

Therefore, the following inequality holds for all vectors $\epsilon \in \mathbb{R}^n$:

$$\|\mathbf{D}\phi_{t_0}^{t_f} \cdot \epsilon\|_2 \leq \exp(\sigma |t_f - t_0|) \|\epsilon\|_2. \tag{5}$$

3 Error analysis of flow map composition

If the dynamical system (1) is time-varying, then it may be necessary to compute a time-series of flow maps, $\phi_{t_0}^{t_0+T}$, at neighboring discrete points in time, $t_0 \in k\Delta t$ for $k \in \mathbb{Z}$, on the same spatial domain. The *fast* FTLE method [21] speeds up neighboring flow map computations by computing and storing intermediate flow maps, $\phi_{t_0}^{t_0+\Delta t}$, which are used to construct longer-time flow maps by composition. For $t_0 = 0$ and $T = N\Delta t$, this becomes:

$$\phi_0^{N\Delta t} = \phi_{(N-1)\Delta t}^{N\Delta t} \circ \cdots \circ \phi_0^{\Delta t}. \tag{6}$$

In practice, we seek the flow map on a discrete set of points, $X_0 \subset \mathcal{D}$. However, the intermediate flow maps, $\phi_{(k-1)\Delta t}^{k\Delta t}$ restricted to X_0 may not map to X_0. For example, if X_0 is a uniform grid, it is unlikely that a flow will map these points to exactly the same grid. Therefore, it is necessary to *interpolate* the grid X_0 through the various flow maps. The quantitative and qualitative effect of interpolation on flow map composition error has been extensively numerically investigated for continuous-time fluid systems, in [21]. However, there is a need for a general error analysis for the flow map composition, which is provided here.

Consider a number of flow maps, ϕ^{t_j} of duration t_j. From (5), we may choose each duration t_j sufficiently small for the following bound to hold:

$$1 \leq \|\mathbf{D}\phi^{t_j}\|_2 = \exp(\sigma|t_j|) < \alpha_j \leq \alpha. \tag{7}$$

Consider the following composition of flow maps, with the addition of some bounded interpolation error, $\epsilon_j \in \mathbb{R}^n$, such that each $\|\epsilon_j\|_2 < \beta \ll 1$:

$$\phi^{t_2}\left(\phi^{t_1}(x) + \epsilon\right) \approx \phi^{t_2}\left(\phi^{t_1}(x)\right) + \mathbf{D}\phi^{t_2}\left(\phi^{t_1}(x)\right) \cdot \epsilon + \mathcal{O}(\epsilon^2). \tag{8}$$

Neglecting higher order terms, the error is $\mathbf{D}\phi^{t_2}\left(\phi^{t_1}(x)\right) \cdot \epsilon < \alpha\beta$. Adding a third flow map, the expression becomes:

$$\phi^{t_3}\left(\phi^{t_2}\left(\phi^{t_1}(x) + \epsilon_1\right) + \epsilon_2\right) \approx \phi^{t_3}\left(\phi^{t_2}\left(\phi^{t_1}(x)\right)\right) + \mathbf{D}\phi^{t_3}\left(\phi^{t_2}\left(\phi^{t_1}(x)\right)\right) \cdot \left[\epsilon_2 + \mathbf{D}\phi^{t_2}\left(\phi^{t_1}(x)\right) \cdot \epsilon_1\right] + \mathcal{O}(\epsilon_i\epsilon_j). \tag{9}$$

Again, the error is given by $\mathbf{D}\phi^{t_3}\left(\phi^{t_2}\left(\phi^{t_1}(x)\right)\right) \cdot \left[\epsilon_2 + \mathbf{D}\phi^{t_2}\left(\phi^{t_1}(x)\right) \cdot \epsilon_1\right] \leq \alpha\beta(\alpha + 1)$. This establishes a recursion. Adding a fourth composition, the error is bounded by $\alpha\beta\left[1 + \alpha + \alpha^2\right]$. For N compositions, the error is bounded by:

$$\frac{\alpha\beta\left(1 - \alpha^{N-1}\right)}{1 - \alpha}. \tag{10}$$

For two-dimensional incompressible flows, the local flow map Jacobian has determinant equal to one, so that the best case scenario is $\alpha = 1$. Thus, there is a lower bound to the error, given by:

$$(N - 1)\beta. \tag{11}$$

This is a reasonable lower bound, since error may accumulate linearly. However, for any region of positive FTLE, $\alpha > 1$, and the expression for the upper bound in Eq. (10) diverges. This is consistent with the observations in [21], where local errors may be amplified by the local finite-time Lyapunov exponent. Fortunately, regions with high local FTLE generally repel particles, so that particles tend to only spend a short amount of time in regions of large positive FTLE.

It is possible to be more careful about the error expression using the errors α_j from Eq. (7):

$$\beta\alpha_N\left(1 + \alpha_{N-1}\left(1 + \alpha_{N-2}\left(\cdots\alpha_3\left(1 + \alpha_2\right)\right)\right)\right). \tag{12}$$

Thus, it is clear that the error will only grow significantly when the exponential stretching is persistent over a long period of time.

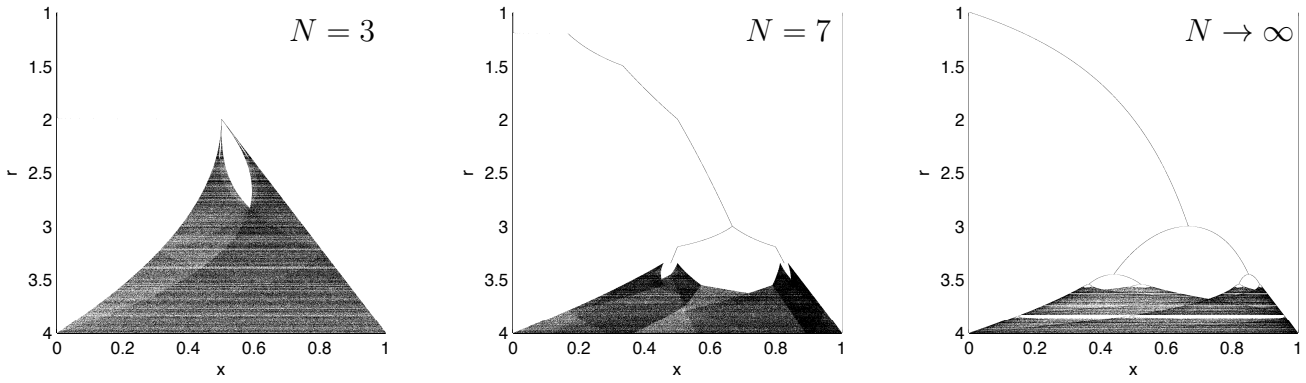

Figure 2: The case of linear interpolation of the logistic map with $N = 3$ interpolation nodes is equivalent to the tent map with half amplitude (left). As the number of linear interpolation nodes increases, additional features are resolved (middle). In the limit as the number of interpolation nodes becomes very large, we recover the exact logistic map (right).

4 Discrete-time dynamical systems

Even for continuous-time dynamical systems, the flow map establishes a discrete-time system. Therefore, it is fruitful to investigate error accumulation from interpolation for the broader class of discrete-time dynamical systems.

As a simple example, consider the logistic map:

$$x_{k+1} = r x_k (1 - x_k), \tag{13}$$

which is given by a quadratic nonlinearity. If three interpolation points are used to approximate the quadratic map, the result is a hat map:

$$x_{k+1} = \begin{cases} \mu x_k, & \text{for} \quad x_k < 1/2 \\ \mu(1 - x_k), & \text{for} \quad x_k \geq 1/2 \end{cases}. \tag{14}$$

Interestingly, as the number of interpolation points increases, additional features of the bifurcation plot appear, although there are remnants of hat maps in the fine details, as shown in Fig. 2. A cubic spline interpolation yields perfect results, even with three points, as the flow map is quite simple. Several other discrete-time systems have been analyzed with similar results.

5 Conclusion

In conclusion, this work has investigated the use of short-time flow map composition and interpolation for the extraction of coherent sets and attracting structures in dynamical systems. In particular, a detailed error analysis of flow map composition illustrates the various types of error and how they manifest, providing both an upper and lower bound. In addition, flow map composition and interpolation is investigated on discrete-time dynamical systems, where it is found that the effect of the order of interpolation is more pronounced than the number of interpolation points. Connecting the error analysis above to more sophisticated flows and to the theoretical error analysis of Ying and Candès for autonomous systems [22], is the subject of ongoing work.

Acknowledgements

I am grateful for discussions with Mark Luchtenburg and Clancy Rowley about flow map composition and finite time Lyapunov exponents. I would like to acknowledge support from the Air Force Office of Scientific Research (AFOSR FA9550-18-1-0200).

References

[1] G. Froyland and K. Padberg. Almost-invariant sets and invariant manifolds – connecting probabilistic and geometric descriptions of coherent structures in flows. *Physica D*, 238:1507–1523, 2009.

[2] G. Haller. Distinguished material surfaces and coherent structures in three-dimensional fluid flows. *Physica D*, 149:248–277, 2001.

[3] G. Haller. Lagrangian coherent structures from approximate velocity data. *Physics of Fluids*, 14(6):1851–1861, June 2002.

[4] S. C. Shadden, F. Lekien, and J. E. Marsden. Definition and properties of Lagrangian coherent structures from finite-time Lyapunov exponents in two-dimensional aperiodic flows. *Physica D*, 212:271–304, 2005.

[5] M. Farazmand and G. Haller. Computing Lagrangian coherent structures from their variational theory. *Chaos*, 22(013128):013128–1–013128–12, 2012.

[6] J. Peng and J. O. Dabiri. The 'upstream wake' of swimming and flying animals and its correlation with propulsive efficiency. *The Journal of Experimental Biology*, 211:2669–2677, 2008.

[7] M. A. Green, C. W. Rowley, and G. Haller. Detection of Lagrangian coherent structures in 3D turbulence. *Journal of Fluid Mechanics*, 572:111–120, 2007.

[8] F. Lekien, C. Coulliette, A. J. Mariano, E. H. Ryan, L. K. Shay, G. Haller, and J. E. Marsden. Pollution release tied to invariant manifolds: a case study for the coast of Florida. *Physica D*, 210:1–20, 2005.

[9] S. C. Shadden and C. A. Taylor. Characterization of coherent structures in the cardiovascular system. *Annals of Biomedical Engineering*, 36(7):1152–1162, 2008.

[10] George Haller and Themistoklis Sapsis. Where do inertial particles go in fluid flows? *Physica D*, 237(5):573–583, 2008.

[11] M Sudharsan, Steven L Brunton, and James J Riley. Lagrangian coherent structures and inertial particle dynamics. *Physical Review E*, 93(3):033108, 2016.

[12] P. Tallapragada and S. D. Ross. Particle segregation by Stokes number for small neutrally buoyant spheres in a fluid. *Physical Review E*, 78:036308–1–036308–9, 2008.

[13] P. Tallapragada, S. D. Ross, and D. G. Schmale III. Lagrangian coherent structures are associated with fluctuations in airborne microbial populations. *Chaos*, 21:033122–1–033122–16, 2011.

[14] Francisco J Beron-Vera, Marıa J Olascoaga, George Haller, Mohammad Farazmand, Joaquın Trinanes, and Yan Wang. Dissipative inertial transport patterns near coherent lagrangian eddies in the ocean. *arXiv preprint arXiv:1408.6512*, 2014.

[15] J. Peng and J. O. Dabiri. Transport of inertial particles by Lagrangian coherent structures: application to predator-prey interaction in jellyfish feeding. *Journal of Fluid Mechanics*, 623:75–84, 2009.

[16] Wenbo Tang, George Haller, Jong-Jin Baik, and Young-Hee Ryu. Locating an atmospheric contamination source using slow manifolds. *Physics of Fluids*, 21(4):043302, 2009.

[17] W. Tang, B. Knutson, A. Mahalov, and R. Dimitrova. The geometry of inertial particle mixing in urban flows, from deterministic and random displacement models. *Physics of Fluids*, 24:063302–1–063302–18, 2012.

[18] Themistoklis Sapsis and George Haller. Inertial particle dynamics in a hurricane. *Journal of the Atmospheric Sciences*, 66(8), 2009.

[19] K. Taira and T. Colonius. The immersed boundary method: a projection approach. *Journal of Computational Physics*, 225(2):2118–2137, 2007.

[20] T. Colonius and K. Taira. A fast immersed boundary method using a nullspace approach and multi-domain far-field boundary conditions. *Computer Methods in Applied Mechanics and Engineering*, 197:2131–2146, 2008.

[21] S. L. Brunton and C. W. Rowley. Fast computation of FTLE fields for unsteady flows: a comparison of methods. *Chaos*, 20:017503, 2010.

[22] L. Ying and E. J. Candès. Fast geodesics computation with the phase flow method. *Journal of Computational Physics*, 220:6–18, 2006.

[23] Dongbin Xiu and George Em Karniadakis. The Wiener-Askey Polynomial Chaos for Stochastic Differential Equations. *SIAM Journal of Scientific Computing*, 24(2):619–644, 2002.

[24] Dongbin Xiu and George Em Karniadakis. Modeling uncertainty in flow simulations via generalized polynomial chaos. *Journal of Computational Physics*, 187(1):137–167, May 2003.

[25] Xiaoliang Wan and George Em Karniadakis. An adaptive multi-element generalized polynomial chaos method for stochastic differential equations. *Journal of Computational Physics*, 209(2):617–642, November 2005.

[26] Marc Gerritsma, Jan-Bart van der Steen, Peter Edward Julia Vos, and George Em Karniadakis. Time-dependent generalized polynomial chaos. *Journal of Computational Physics*, 229(22):8333–8363, November 2010.

[27] D. M. Luchtenburg, S. L. Brunton, and C. W. Rowley. Long-time uncertainty propagation using generalized polynomial chaos and flow map composition. *Journal of Computational Physics*, 274:783–802, 2014.